Efficient model of evolution of wear in quasi-steady-state sliding contacts

Jakub Lengiewicz*, Stanisław Stupkiewicz

Institute of Fundamental Technological Research (IPPT)
Pawińskiego 5B, 02–106 Warsaw, Poland

Abstract

A computationally efficient model of evolution of contact and wear is developed for a general periodic pin-on-flat problem with the focus on the pin-on-disc configuration and Archard wear model. The evolving contact state is assumed to be fully controlled by the wear process except during a short initial transient period controlled by both wear and elasticity. The contact pressure distribution is thus obtained by considering only the local wear model and the geometry of the conforming contact, without referring to the underlying elasticity problem. Evolution of the contact state is then obtained by time integration of the resulting rate-problem, and two computational schemes are developed for that purpose employing either the forward- or the backward-Euler method. The model is successfully verified against a three-dimensional finite element model. A dimensionless wear-mode index specifying the relative magnitude of wear coefficients of the contact pair is introduced, and model predictions are presented as a function of this parameter.

Keywords: contact mechanics, wear, simulation, quasi-steady-state process, rigid-wear model, pin-on-disc

1. Introduction

The wear phenomenon is well known for its high complexity and sensitivity to tribological conditions, and a variety of micro-scale mechanisms

*Corresponding author. Email address: jleng@ippt.gov.pl, phone: (+48) 22 826 12 81

inducing macroscopic loss of material at the contact surface have been identified and analysed. However, general predictive models of wear are still missing, and the simple model of Archard [1] is still the most popular wear model, commonly used in computational practice.

Simulation of progressive wear and associated evolution of contact conditions is also a challenging task. The general methodology amounts to solving a contact problem for a fixed geometry of contacting members and subsequently updating the geometry, all in an incremental manner. Computational approaches employing the finite element method [2–7], the boundary element method [8–10], or specialized contact solvers [11, 12] have been developed for that purpose. The geometry is usually updated according to an explicit forward-Euler time integration scheme. This scheme is known to be conditionally stable, and the critical time increment decreases with increasing elastic modulus and with decreasing element size, cf. [2]. A large number of time steps is thus usually needed to avoid instability of the numerical scheme, therefore the overall computational cost is high.

In an attempt to reduce the computational cost, simplified approaches are also developed. For instance, the Winkler model is used to determine the contact pressures in [13], and an elliptical contact area and constant pressure are explicitly assumed in the incremental scheme proposed in [5].

Several approaches have also been developed which consider asymptotic states or steady-state regimes reached in the course of the wear process. A minimization approach is developed in [14] to obtain the worn-out geometry in the asymptotic state under cyclic loading. The formulation includes the elastic response, and it relies on the Green functions for the worn-out half-plane. In [15, 16], optimal shapes are determined for steady-state sliding wear processes using the concept of uniform wear over the contact surface. The approach is further developed in [17] for the case of reciprocating contacts. Asymptotic modeling of reciprocating sliding wear is presented in [18, 19], and, in the resulting model, it is assumed that the contact pressure is uniform and that the contact area is elliptic.

In this work, a highly efficient model of evolution of contact and wear is developed for a general periodic pin-on-flat wear problem. This class of problems includes, for instance, the popular pin-on-disc and reciprocating pin-on-flat configurations. It is assumed that the evolving contact state is fully controlled by the wear process so that the elastic deflections do not influence the contact pressure and the wear process. Accordingly, the contact pressure distribution is obtained by considering only the local wear model

and the geometry of the conforming contact, without referring to the underlying elasticity problem. Evolution of the contact state is then obtained by time integration of the resulting rate-problem, and two computational schemes are developed for that purpose employing either the forward- or the backward-Euler method. In particular, the evolving shape of the contact zone is obtained from the model without any additional assumptions. This is a distinctive feature of the present model as compared to other simplified approaches. The model is successfully verified against a full three-dimensional finite-element simulation.

The model considers the general case of both contacting bodies subjected to wear. It is shown that the wear problem formulated in terms of dimensionless quantities depends on a single dimensionless parameter, called the wear-mode index, which specifies the relative magnitude of the wear coefficients of the contact pair.

The paper is organized as follows. In Section 2, the model is introduced, and its special form corresponding to the Archard wear model is derived. Solution schemes, including spatial and temporal discretization, are discussed in Section 3. A study of the predictions of the model is presented in Section 4, including a comparison to the three-dimensional finite element model. In the Appendix, the computer implementation of the model is briefly commented, and the corresponding *Mathematica* code is provided as a supplementary material accompanying this paper.

2. Model of wear-controlled quasi-steady-state sliding contacts

2.1. Assumptions

Wear due to repeated contact and frictional sliding occurs in various tribological pairs. This includes some commonly used tribological test configurations, such as the pin-on-disc, reciprocating pin-on-flat, and pin-on-cylinder tribological tests. Each of these configurations can be classified as a *periodic pin-on-flat wear problem*, cf. Fig. 1. Various pin shapes can also be used in these tests (spherical, cylindrical, conical, etc.). To fix the attention, in this work we shall mostly refer to the spherical pin-on-disc configuration, but the approach is more general and applies to other configurations as well.

Consider contact and wear of two elastic bodies in the periodic pin-on-flat configuration. The contact surfaces are initially non-conforming (point contact); however, as the bodies are worn during the initial period, a *conforming contact* develops in the actual contact zone, i.e., between the wear groove on

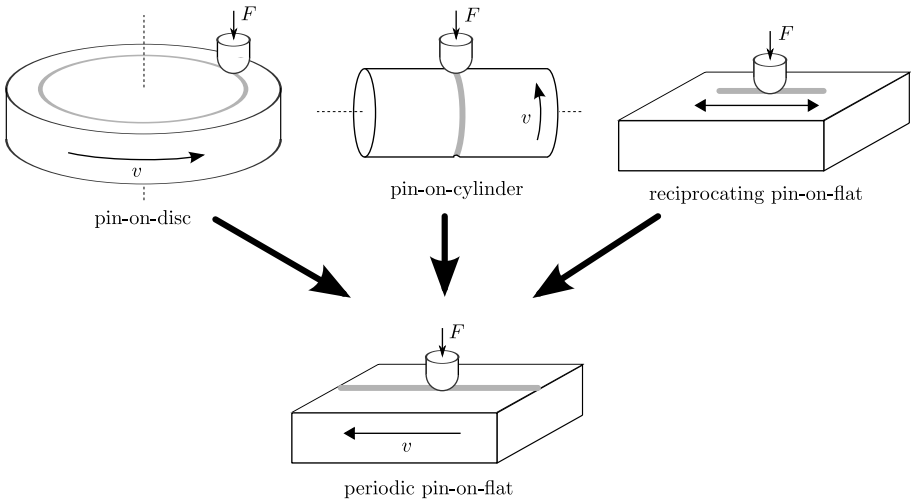

Figure 1: Three commonly used tribological tests and their simplified representation.

the disc and the wear scar on the ball, and further evolves during the wear process.

Wear processes are usually slow. Two time scales can thus be introduced [7]: the fast time of the deformation (contact) problem and the slow time related to shape evolution due to wear. Referring to the pin-on-disc test, the fast time corresponds to one revolution of the disc, while the observable wear processes occur at the slow time scale as a result of accumulation of wear over multiple revolutions. Accordingly, the deformation and shape evolution processes can be partially decoupled [7]. In the present context, the deformation problem can thus be treated as a strictly periodic contact problem in which the shape changes due to wear over one cycle are negligible.

The wear problem corresponding to the pin-on-disc (or pin-on-cylinder) configuration can actually be classified as a *quasi-steady-state wear* process, cf. [16, 7], meaning that if the shape evolution due to wear was temporarily suppressed then the contact problem would be a steady-state problem (in the frame attached to the ball). In a quasi-steady-state wear process, the contact pressure is thus constant in the fast time scale, though it may evolve in the slow time scale as a result of wear-induced changes of the contact area.

As it is shown in subsequent sections, the shape changes due to wear and the associated evolution of contact pressures can be determined by considering only the wear model and the kinematics of the progressive wear process. Elastic deformations are thus not considered, and the usual contact prob-

lem is not solved. This requires an additional assumption that the elastic deflections are small compared to the shape changes due to wear. This is a typical situation, for instance, in the case of metallic or ceramic contacts. In this sense, the contacting bodies are treated as rigid, and the model will be referred to as *the rigid-wear model*.

The present model considers the general case when both contacting bodies wear away, i.e. both the wear scar on the pin and the wear groove on the disc form and evolve during the wear process. The situation when the disc does not wear away is a trivial special case. At the same time, the present model is not directly applicable in the other limiting case when the pin does not wear away: the shape of the wear groove is then trivially predicted (assuming the elastic deflections are negligible), but neither the contact pressures nor the contact zone can be determined without solving the complete contact and wear problem.

Two additional technical assumptions are also adopted in the present model. It is assumed that the normal to the pin surface is not affected by the wear process (i.e., the slope of the wear groove is assumed small), and the disc is assumed to be homogeneous along the sliding direction.

2.2. Geometry of the conforming contact zone

Consider a contact and wear problem in the pin-on-disc configuration, where both the pin and the disc are subjected to wear. In the following, a spherical pin of the radius R is considered, but other pin shapes could also be considered. The pin is pressed down with the force F onto the disc rotating with a constant angular velocity $\omega = 2\pi/\Delta\tau$. The coordinate system is attached to the ball with the x-axis along the sliding direction and the z-axis normal to the disc surface.

The length of the circular sliding path of the diameter d is $S = \pi d$. For sufficiently large d, the curvature of the sliding path can be neglected, so that a linear relative motion with velocity $v = S/\Delta\tau$ is considered. In order to adequately represent the repeated contact due to rotation of the disc, the length of the flat along the sliding path is taken equal to S, cf. Fig. 2.

As explained above, the wear process is assumed to be slow. This implies that the evolving shape of the wear groove on the disc is uniform along the sliding direction x, and it is fully represented by the profile $w_d(y,t) \geq 0$ along the perpendicular direction.

The wear profile of the ball is denoted by $w_b(x,y,t) \geq 0$. As the elastic deflections are neglected and conforming contact is assumed in the contact

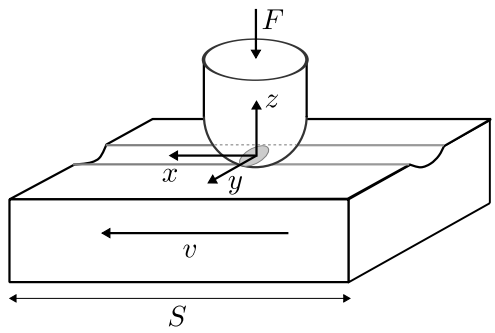

Figure 2: Periodic ball-on-flat problem: periodic cell of length S with the wear groove along the sliding direction x, and the contact zone (gray ellipse in the middle).

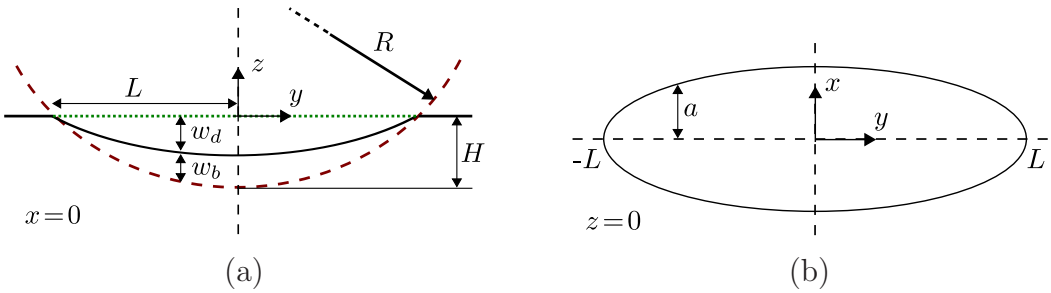

Figure 3: Geometry of the conforming contact zone: (a) central cross-section perpendicular to the sliding direction, (b) projection of the wear scare (contact zone) onto the (x, y)-plane.

zone, the following geometrical constraint holds,

$$w_d(y,t) + w_b(x,y,t) = \max(0, \sqrt{R^2 - x^2 - y^2} - R + H(t)), \tag{1}$$

where $H(t)$ is the overall approach in the normal direction, cf. Fig. 3a.

The contact zone is a region in which $w_b > 0$. The length of the contact zone along the x-direction is $2a(y,t)$, so that $|x| \leq a(y,t)$ in the contact zone, cf. Fig. 3b, where

$$a(y,t) = \sqrt{R_*^2(y) - (R_*(y) - w_b^0(y,t))^2}, \tag{2}$$

and $w_b^0(y,t) = w_b(0,y,t)$. Here, $R_*(y)$ denotes the radius of the section of the ball by the plane $y = \text{const}$,

$$R_*(y) = \sqrt{R^2 - y^2}. \tag{3}$$

The width of the contact zone along the y-direction is $2L(t)$, where

$$L(t) = \sqrt{R^2 - (R - H(t))^2}. \tag{4}$$

As already discussed, the wear groove is uniform along the sliding direction, and conforming contact is assumed. Thus, the wear profile of the ball $w_b(x, y, t)$ is explicitly determined by the wear profile $w_b^0(y, t)$ at $x = 0$,

$$w_b(x, y, t) = \sqrt{R^2 - x^2 - y^2} - R_*(y) + w_b^0(y, t) \quad \text{for} \quad |x| \leq a(y, t). \tag{5}$$

Moreover, it follows from (5) that the wear rate $\dot{w}_b$ is uniform along the sliding direction, so that

$$\dot{w}_b(x, y, t) = \dot{w}_b^0(y, t) \quad \text{for} \quad |x| \leq a(y, t). \tag{6}$$

The geometrical constraint (1) can now be equivalently specified at $x = 0$, i.e., in terms of the y-coordinate only,

$$w_d(y, t) + w_b^0(y, t) = \max(0, \sqrt{R^2 - y^2} - R + H(t)). \tag{7}$$

Equation (7) implies the following relationship for the wear rates:

$$\dot{w}_d(y, t) + \dot{w}_b^0(y, t) = \begin{cases} \dot{H} & \text{for } |y| \leq L(t), \\ 0 & \text{elsewhere.} \end{cases} \tag{8}$$

2.3. Quasi-steady-state wear problem

As discussed in Section 2.1, two time scales are introduced. The instantaneous wear rate at the fast time scale τ is governed by a suitable wear model, e.g., the Archard wear model to be discussed later. The resulting instantaneous local wear rates of the ball and the disc are denoted by $\dot{\tilde{w}}_b(x, y, \tau)$ and $\dot{\tilde{w}}_d(x, y, \tau)$, respectively. The wear rate at the slow time scale t is then obtained by averaging the instantaneous wear rates over the characteristic time interval $\Delta\tau$, e.g., one revolution of the disc, cf. [7].

The assumption of separation of the two time scales implies that the shape changes due to wear and the related variation of the contact pressure are suppressed at the fast time scale. As a result, the geometry of the conforming contact zone and the pressure are constant upon averaging of the instantaneous wear rates.

Averaging of the wear rate of the disc is performed at a fixed material point, i.e., at $(x', y') = (x - v\tau, y)$,

$$\begin{aligned} \dot{w}_d(y,t) &= \frac{1}{\Delta\tau} \int_t^{t+\Delta\tau} \dot{\tilde{w}}_d(x', y', \tau)\,\mathrm{d}\tau = \frac{1}{\Delta\tau} \int_0^S \dot{\tilde{w}}_d(x,y,t) \frac{\mathrm{d}x}{v} \\ &= \frac{1}{S} \int_{-a(y,t)}^{a(y,t)} \dot{\tilde{w}}_d(x,y,t)\,\mathrm{d}x, \end{aligned} \tag{9}$$

in view of $\dot{\tilde{w}}_d(x,y,t) = 0$ for $|x| > a(y,t)$. The time integration has thus been replaced by integration along the sliding path, cf. [12]. As concluded in Section 2.2, the wear groove is uniform along the sliding direction, and this is adequately represented by Eq. (9).

In case of the ball, we have simply

$$\dot{w}_b(x,y,t) = \frac{1}{\Delta\tau} \int_t^{t+\Delta\tau} \dot{\tilde{w}}_b(x,y,\tau)\,\mathrm{d}\tau = \dot{\tilde{w}}_b(x,y,t). \tag{10}$$

In view of Eq. (6), the averaged wear rate of the ball is also uniform along the sliding direction, so that conforming contact between the ball and the disc is maintained. This implies that the instantaneous wear rate $\dot{\tilde{w}}_b(x,y,t)$ does not depend on x. This property is exploited in Section 2.4.

The wear model provides a constitutive relationship between the local wear rate and the contact pressure, sliding velocity, and, possibly, other parameters, namely

$$\dot{\tilde{w}}_\alpha = k_\alpha(p, v, \ldots) p v, \tag{11}$$

where $p = p(x,y,t)$ denotes the contact pressure, v is the sliding velocity, and index $\alpha = \{b, d\}$ indicates the ball or the disc. The wear coefficient $k_\alpha(p, v, \ldots)$ may in general depend on the contact pressure, sliding velocity, etc. The classical Archard wear model is recovered when the wear coefficient is a constant parameter.

The model is completed by specifying the force-balance equation,

$$F = \int_{-L(t)}^{L(t)} \int_{-a(y,t)}^{a(y,t)} p(x,y,t)\,\mathrm{d}x\mathrm{d}y, \tag{12}$$

where F is the total normal force.

Equations (8), (9), (10), (11) and (12) constitute the set of equations for the unknown contact pressure $p(x, y, t)$, wear profiles $w_b^0(y, t)$ and $w_d(y, t)$, and normal displacement $H(t)$ of the ball. Additionally, quantities $a(y, t)$ and $L(t)$ are specified by Eqs. (2) and (4), respectively. We note that these equations define the wear problem at the slow time scale without referring to the fast time scale. Specification of the initial conditions is postponed to Section 3.

Remark 1. The present rigid-wear model has been developed under the assumption that the elastic deflections are negligible so that the evolution of the system is fully described in terms of the actual (conforming) geometry of the surfaces. Clearly, this assumption is not valid during the initial stage of the wear process when contact evolves from purely elastic to wear-controlled contact conditions. Analysis of this initial stage is carried out in Section 4.1.

2.4. Archard wear model

In this section, the model is analyzed in detail for the special case of the classical Archard wear model with a constant wear coefficient. The wear model (11) now reads

$$\dot{\tilde{w}}_b(x, y, t) = k_b v p(x, y, t), \qquad \dot{\tilde{w}}_d(x, y, t) = k_d v p(x, y, t), \tag{13}$$

where k_b and k_d are constant parameters. In view of Eqs. (10) and (6), the wear rate $\dot{\tilde{w}}_b$ is constant along the sliding direction, i.e., it does not depend on x. Thus, the local wear model specified for the ball, cf. Eq. $(13)_1$, implies that also the pressure p is constant along the sliding direction x, and so is the wear rate $\dot{\tilde{w}}_d$, in view of Eq. $(13)_2$. Equation (13) is thus rewritten in the form

$$\dot{\tilde{w}}_b(y, t) = k_b v p(y, t), \qquad \dot{\tilde{w}}_d(y, t) = k_d v p(y, t), \tag{14}$$

which is valid in the contact zone $|x| \leq a(y, t)$.

The important conclusion is that only one spatial dimension is involved in the problem at hand. In particular, time averaging in Eq. (9) simplifies to

$$\dot{w}_d(y, t) = \frac{2a(y, t)}{S} k_d v p(y, t), \tag{15}$$

while the wear rate of the ball is specified by

$$\dot{w}_b^0(y, t) = k_b v p(y, t). \tag{16}$$

By combining Eqs. (15), (16) and (8), the following relationship between the contact pressure p and $\dot{H}$ is obtained:

$$p(y,t) = \frac{\dot{H}(t)}{v}\left(k_b + \frac{2a(y,t)}{S}\,k_d\right)^{-1}, \tag{17}$$

while $\dot{H}$ depends on the total force F through the force-balance equation (12),

$$\dot{H}(t) = Fv\left[\int_{-L(t)}^{L(t)} 2a(y,t)\left(k_b + \frac{2a(y,t)}{S}\,k_d\right)^{-1}\mathrm{d}y\right]^{-1}. \tag{18}$$

The structure of the *rate-problem* defined above is thus the following. Consider a typical time instant $t = t'$ at which the geometry of the conforming contact zone is known. This is uniquely defined by specifying, for instance, $H(t')$ and $w_d(y,t')$, while the remaining quantities, such as $L(t')$, $a(y,t')$ and $w_b^0(y,t')$, are determined by the relationships provided in Section 2.2. Then, the rate $\dot{H}(t')$ and the pressure $p(y,t')$ are given by Eqs. (18) and (17), respectively, and the wear rates $\dot{w}_d(y,t')$ and $\dot{w}_b^0(y,t')$ are given by Eqs. (15) and (16).

In short, the wear rates at $t = t'$ depend solely on the contact geometry at $t = t'$. Evolution of the contact geometry results then from time integration of this relationship. Integration schemes suitable for the present rate-problem are discussed in Section 3.

Note that the present model predicts the contact pressure and its evolution without referring to the underlying elasticity problem. The pressure profile along the y-axis follows from Eq. (17) and is sketched in Fig. 4, where $p_{max} = \dot{H}/(vk_b)$ and $\bar{a}_0 = a(0,t)/R$, and we have $a(L,t) = 0$. Additionally, a dimensionless parameter, denoted by I_w and called the *wear-mode index*,

$$I_w = \frac{Rk_d}{Sk_b}, \tag{19}$$

has been introduced. This parameter indicates the relative magnitude of the wear coefficients of the contact pair.

Remark 2. The above rate-problem is singular for $H = L = 0$: it follows from Eq. (18) that $\dot{H}$ is infinite for $L = 0$. When formulating the initial conditions, this must be taken into account in addition to the physical relevance discussed in Remark 1.

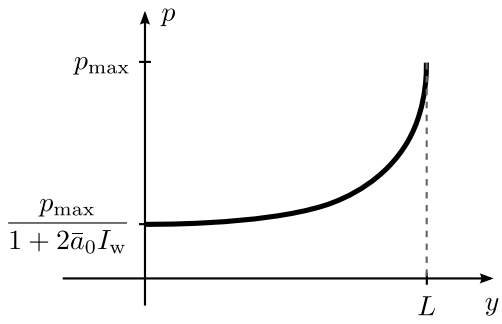

Figure 4: Pressure distribution along the y-direction (schematic).

2.5. Dimensionless quantities

Let us introduce the following dimensionless quantities:

$$\begin{aligned} \bar{S} &= \frac{S}{R}, \qquad \bar{y} = \frac{y}{R}, \qquad \bar{w}_d = \frac{w_d}{R}, \qquad \bar{w}_b^0 = \frac{w_b^0}{R}, \\ \bar{L} &= \frac{L}{R}, \qquad \bar{a} = \frac{a}{R}, \qquad \bar{t} = \frac{t}{t^*}, \qquad \bar{p} = \frac{p}{p^*}, \end{aligned} \tag{20}$$

where

$$t^* = \frac{R^3}{k_b F v}, \qquad p^* = \frac{F}{R^2}. \tag{21}$$

The rate-problem (15)-(18) can now be expressed in a dimensionless form, viz.

$$\dot{\bar{H}} = \left[\int_{-\bar{L}}^{\bar{L}} 2\bar{a} \left(1 + 2I_w \bar{a}\right)^{-1} \mathrm{d}\bar{y} \right]^{-1}, \qquad \bar{p} = \left(1 + 2I_w \bar{a}\right)^{-1} \dot{\bar{H}}, \tag{22}$$

and

$$\dot{\bar{w}}_b^0 = \bar{p}, \qquad \dot{\bar{w}}_d = 2I_w \bar{a} \bar{p}, \tag{23}$$

where the time derivatives of the dimensionless quantities are taken with respect to the dimensionless time $\bar{t}$, and the wear-mode index I_w is given by Eq. (19).

3. Solution method

The governing equations of the problem are solved incrementally at distinct time instants t_n, $n = 1, \ldots, N_{max}$. Due to the fact that the boundary $L(t)$ of the contact zone increases during the wear process, a special

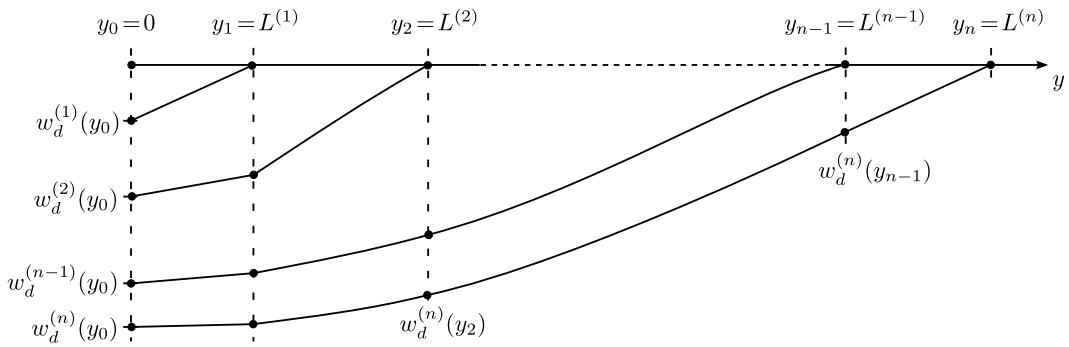

Figure 5: Discretized wear profiles of disc. Spatial discretization follows the boundary of the contact zone.

form of spatial discretization is proposed in order to follow this boundary. At every time step t_n, a new spatial point is added on the boundary at the position $L^{(n)} = L(t_n)$, cf. Fig. 5. Due to symmetry, only the $y \geq 0$ half-plane is considered. At $t = t_n$, there are thus $n + 1$ spatial points, $y_0 = 0, y_1 = L^{(1)}, \ldots, y_n = L^{(n)}$, at which the evolution equations are solved.

In the following, the case of the Archard wear model is only considered. However, the presented methods, especially the implicit scheme, can be easily extended to other, more complicated wear laws. For example, one can consider pressure-dependent wear coefficients $k_b(p)$ and $k_d(p)$, and the structure of the incremental problem remains the same.

3.1. Explicit forward-Euler time integration scheme

At a typical time step $t = t_n$, the wear profiles of the ball $w_b^{(n)}(y_i)$ and of the disc $w_d^{(n)}(y_i)$ are assumed known for $i = 0, \ldots, n$. Also the overall normal displacement of the ball $H^{(n)}$ is known, and the quantities $L^{(n)}$ and $a^{(n)}(y_i)$ follow from Eqs. (2) and (4).

We introduce an auxiliary quantity,

$$\hat{p}^{(n)}(y_i) := \left(k_b + \frac{2a^{(n)}(y_i)}{S} k_d \right)^{-1}, \tag{24}$$

and by applying the trapezoidal integration rule to Eq. (18), the following expression for $\dot{H}^{(n)}$ is obtained:

$$\dot{H}^{(n)} := Fv \left[2 \sum_{i=0}^{n-1} (y_{i+1} - y_i)(a^{(n)}(y_i)\hat{p}^{(n)}(y_i) + a^{(n)}(y_{i+1})\hat{p}^{(n)}(y_{i+1})) \right]^{-1}. \tag{25}$$

The contact pressures (17) are then straightforwardly recovered:

$$p^{(n)}(y_i) := \frac{\dot{H}^{(n)}}{v}\,\hat{p}^{(n)}(y_i), \tag{26}$$

and the wear rates are obtained from Eqs. (15) and (16):

$$\dot{w}_d^{(n)}(y_i) := \frac{2a^{(n)}(y_i)}{S}\,k_d v p^{(n)}(y_i), \qquad \dot{w}_b^{(n)}(y_i) := k_b v p^{(n)}(y_i), \tag{27}$$

for $i = 0, \ldots, n$.

Now, the explicit forward-Euler time integration rule is applied to compute the wear profiles at time $t_{n+1} = t_n + \Delta t_n$:

$$w_d^{(n+1)}(y_i) := w_d^{(n)}(y_i) + \Delta t_n \dot{w}_d^{(n)}(y_i), \tag{28}$$

$$w_b^{(n+1)}(y_i) := w_b^{(n)}(y_i) + \Delta t_n \dot{w}_b^{(n)}(y_i), \tag{29}$$

for $i = 0, \ldots, n$, and to compute the normal displacement of the ball:

$$H^{(n+1)} := H^{(n)} + \Delta t_n \dot{H}^{(n)}. \tag{30}$$

Subsequently, a new node $y_{n+1} := L^{(n+1)}$ is added to the spatial discretization, where $L^{(n+1)}$ depends on $H^{(n+1)}$ through Eq. (4), and $w_d^{(n+1)}(y_{n+1}) := 0$ and $w_b^{(n+1)}(y_{n+1}) := 0$ are set to fulfill the geometrical constraint (7).

We note that solution of the above incremental problem proceeds by sequential evaluation of the formulas (24)–(30), and no system of equations is solved, which is typical for explicit schemes. Accordingly, the scheme is computationally highly efficient and its computer implementation is straightforward, see the Appendix and the code in *Mathematica* (www.wolfram.com) provided as a supplementary material. However, numerical experiments show that it does not perform well when the depth of the wear scar on the ball is small compared to the depth of the wear groove (i.e., for large wear-mode index I_w). Accordingly, an implicit scheme has been developed which is more complex but is free of the deficiencies of the explicit scheme.

Initial conditions. The initial conditions are specified by assuming that the disc does not wear away during the very first time increment between $t = 0$ and $t = t_1$ (the rate-problem is singular for $H = L = 0$, cf. Remark 2, so that the incremental solution cannot start at $t = 0$). To justify this assumption we note that the contact zone length a is initially small compared to S, cf.

Eq. (27). The radius r_{ini} of the initial wear scar and the approach of the ball $H^{(1)}$ are related by

$$r_{ini} = a^{(1)}(y_0) = L^{(1)} = \sqrt{R^2 - (R - H^{(1)})^2}, \tag{31}$$

and the corresponding initial time instant t_1 follows from the Archard wear model,

$$t_1 := \frac{V_{ini}}{k_b F v}, \qquad V_{ini} := \frac{1}{6}\pi H^{(1)}(3r_{ini}^2 + (H^{(1)})^2). \tag{32}$$

The initial conditions are then prescribed as follows:

$$\begin{aligned} &y_0 := 0, && w_b^{(1)}(y_0) := H^{(1)}, && w_d^{(1)}(y_0) := 0, \\ &y_1 := r_{ini}, && w_b^{(1)}(y_1) := 0, && w_d^{(1)}(y_1) := 0, \end{aligned} \tag{33}$$

and the incremental scheme (24)–(30) proceeds for $n = 1, 2, \ldots$

3.2. Implicit backward-Euler time integration scheme

The quantities $w_b^{(n-1)}(y_i)$, $w_d^{(n-1)}(y_i)$ and $H^{(n-1)}$ are assumed known at the previous time step $t = t_{n-1}$. In order to solve the incremental problem at the current time step $t_n = t_{n-1} + \Delta t_n$, the following set of unknowns is introduced: $\dot{H}^{(n)}$, $\dot{w}_b^{(n)}(y_i)$ for $i = 0, \ldots, n-1$, and $p^{(n)}(y_i)$ for $i = 0, \ldots, n$. The backward-Euler scheme yields then the following update formulas:

$$\begin{aligned} &w_d^{(n)}(y_i) := w_d^{(n-1)}(y_i) + \Delta t_n(\dot{H}^{(n)} - \dot{w}_b^{(n)}(y_i)), && i = 0, \ldots, n-1, \\ &w_b^{(n)}(y_i) := w_b^{(n-1)}(y_i) + \Delta t_n \dot{w}_b^{(n)}(y_i), && i = 0, \ldots, n-1, \\ &H^{(n)} := H^{(n-1)} + \Delta t_n \dot{H}^{(n)}. \end{aligned} \tag{34}$$

Additionally, according to Eq. (7), we have

$$w_b^{(n)}(y_n) := 0, \qquad w_d^{(n)}(y_n) := 0, \tag{35}$$

where $y_n := L^{(n)}$, and $L^{(n)}$ depends on $H^{(n)}$ through Eq. (4).

Now, the following set of $2n + 2$ non-linear equations is constructed:

$$\begin{aligned} &\dot{H}^{(n)} = v\left(k_b + k_d \frac{2a^{(n)}(y_i)}{S}\right) p^{(n)}(y_i), && i = 0, \ldots, n, \\ &\dot{w}_b^{(n)}(y_i) = v k_b p^{(n)}(y_i), && i = 0, \ldots, n-1, \\ &F = 2\sum_{i=0}^{n-1}(y_{i+1} - y_i)(a^{(n)}(y_i)p^{(n)}(y_i) + a^{(n)}(y_{i+1})p^{(n)}(y_{i+1})), \end{aligned} \tag{36}$$

which is then solved simultaneously for all unknowns. Here, $a^{(n)}(y_i)$ are given explicitly by Eq. (2).

The set of equations (36) is non-linear because $a^{(n)}(y_i)$ depend nonlinearly on $\dot{w}_b^{(n)}(y_i)$, and y_n depends nonlinearly on $\dot{H}^{(n)}$. These nonlinear equations are solved numerically, e.g., using the iterative Newton scheme. The computational cost of a single time increment is thus higher compared to the explicit scheme; however, the computations can be carried out with larger time steps. Computer implementation in *Mathematica* is commented in the Appendix, see also the supplementary material, and the present implicit scheme is used in the computations reported in Section 4.

Initial conditions. Contrary to explicit scheme of Section 3.1, the initial conditions are prescribed at time $t_0 = 0$ with no additional assumptions:

$$y_0 := 0, \qquad w_b^{(0)}(y_0) := 0, \qquad w_d^{(0)}(y_0) := 0, \qquad H^{(0)} := 0, \tag{37}$$

and the incremental scheme (34)–(36) proceeds for $n = 1, 2, \ldots$

4. Predictions of the rigid-wear model

4.1. Comparison with a 3D finite element model

In this subsection, the predictions of the rigid-wear model are compared to the results of a full 3D finite element model for a realistic pin-on-disc setup. The aim is to study the transition from the elastic to wear-controlled contact conditions and to check the range of validity of the present model.

The approach to finite element modelling of progressive wear is quite standard [4–7]. The contact and wear problem is solved incrementally. At each time step, the frictional contact problem is first solved, and the wear rate is computed as a postprocessing quantity. The positions of the contact nodes are then updated by integrating the wear rates using the explicit forward-Euler scheme. Finally, the mesh is remapped to the new shape by solving an auxiliary elasticity problem. The present finite element implementation is a 3D extension of that presented in [7]. It employs a general 3D multi-body, finite-deformation contact formulation, and the computer implementation relies on the automation capabilities of the *AceGen/AceFEM* package (http://www.fgg.uni-lj.si/symech/), see [20, 21].

In the finite element model, the disc is analyzed in a fixed Eulerian frame so that, for a given geometry of the wear scar and groove, the frictional

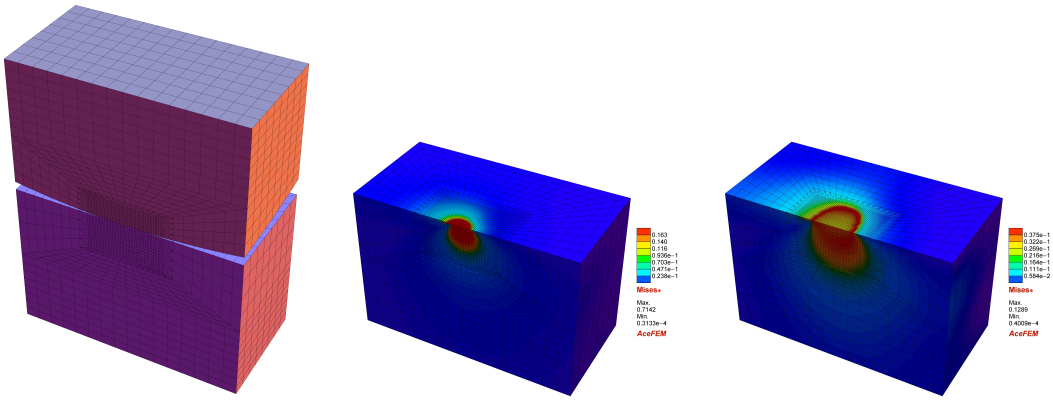

(a) (b) (c)

Figure 6: Three-dimensional model: (a) finite element mesh; (b) equivalent stress σ_{eq} in the disc at the initial time and (c) after 5000 cycles (for $F = 20$ N).

contact problem is a steady-state problem. Accordingly, the shape change of the ball is applied directly at each contact node, whereas the shape of the disc is updated such that the wear groove is uniform along the sliding direction in agreement with the averaging rule (9).

The geometry of the finite element model corresponds to the arrangement presented in Fig. 2. In order to reduce the computational cost, the half-space $y \geq 0$ is only analyzed (symmetry), and the finite element mesh is refined in the vicinity of the contact zone, cf. Fig. 6a. The total number of unknowns is 147881.

The adopted material parameters correspond to a sapphire ball of the radius $R = 3$ mm slid on a steel disc at the diameter $d = 20$ mm, cf. Table 1. In order to illustrate the influence of elastic strains on wear evolution, the computations have been performed for two loading forces: $F = 2$ N and $F = 20$ N. In the case of $F = 20$ N, the wear coefficients have been reduced by the factor of 10 so that the same total wear volume is obtained in both load cases for a given number of cycles (revolutions of disc). The computations are carried out up to 5000 cycles. The corresponding maximum wear depth is 1–1.5 μm so this can be considered as an initial phase of the wear process.

The Hertz contact radius is $a = 31$ μm for $F = 2$ N and $a = 67$ μm for $F = 20$ N, and the maximum Hertz pressure is $p_{max} = 0.99$ GPa and $p_{max} = 2.14$ GPa, respectively. Both features are well represented by the finite element solution at the initial time instant, cf. Fig. 7. The size of the

Table 1: Parameters used in the simulation of the pin-on-disc test.

	Load case #1	Load case #2
Radius of the ball, R	3 mm	—
Sliding path length per one cycle, S	20π mm	—
Young's modulus of the ball, E_b	400 GPa	—
Young's modulus of the disc, E_d	210 GPa	—
Poisson's ratio of the ball, ν_b	0.3	—
Poisson's ratio of the disc, ν_d	0.3	—
Friction coefficient, μ	0.3	—
Normal force, F	2 N	20 N
Wear coefficient of the ball, k_b	2.5×10^{-11} mm^2/N	2.5×10^{-12} mm^2/N
Wear coefficient of the disc, k_d	2.5×10^{-8} mm^2/N	2.5×10^{-9} mm^2/N

mesh in the contact zone is 6.25×6.25 μm so that there are about 5 elements along the initial contact radius for $F = 2$ N and more than 10 elements for $F = 20$ N.

Evolution of the contact pressure, as predicted by the finite element model, is presented in Fig. 7. Distribution of the contact pressure is initially of Hertzian type and it evolves towards the distribution predicted by the rigid-wear model. In the case of $F = 2$ N, the wear-controlled contact conditions are attained at about 2500 cycles: the pressure is constant along the sliding direction, and in the transverse direction the characteristic peak at the end of the contact zone is observed. This is confirmed in Fig. 8 in which the contact pressures predicted by the two models are directly compared for 1200, 2500 and 5000 cycles. It is seen that already at 1200 cycles, the rigid-wear model gives reasonable predictions of the contact zone and pressure. For 2500 and 5000 cycles, the agreement is very good except the peak pressure. Also the wear profiles corresponding to 1200, 2500 and 5000 cycles match perfectly, cf. Fig. 9.

In the case of the higher force $F = 20$ N, the elastic strains are higher and the transient stage is longer. It is seen from Fig. 7c,d that the wear-controlled contact conditions are not fully reached after 5000 cycles. However, the character of pressure evolution is similar to that observed for $F = 2$ N. The wear profiles predicted by the two models show some discrepancy, cf. Fig. 10 which, however, diminishes with the progress of the wear process.

The general conclusion of this subsection is that the assumptions of the rigid-wear model indeed hold after a short transient period. For the normal

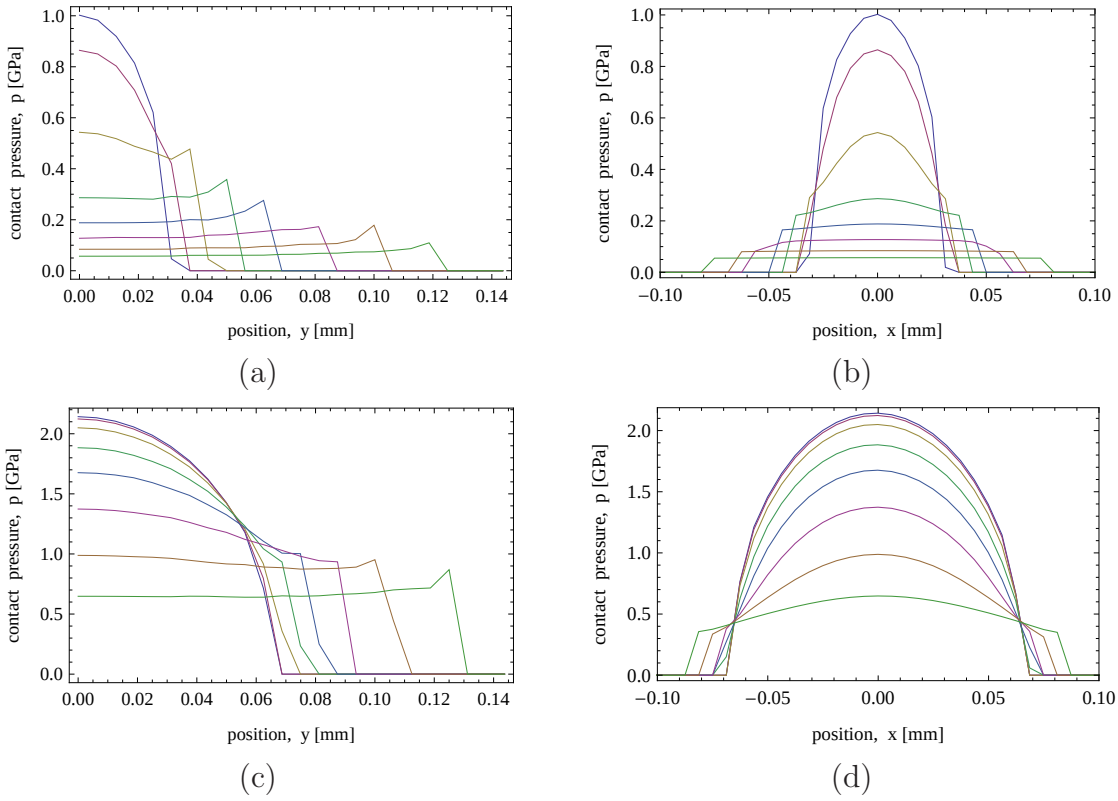

Figure 7: Evolution of contact pressure in the 3D finite element model for $F = 2$ N (a,b) and $F = 20$ N (c,d). Contact pressure profiles at $x = 0$ (a,c) and at $y = 0$ (b,d) are shown. Successive profiles correspond to 0, 20, 100, 300, 600, 1200, 2500 and 5000 cycles.

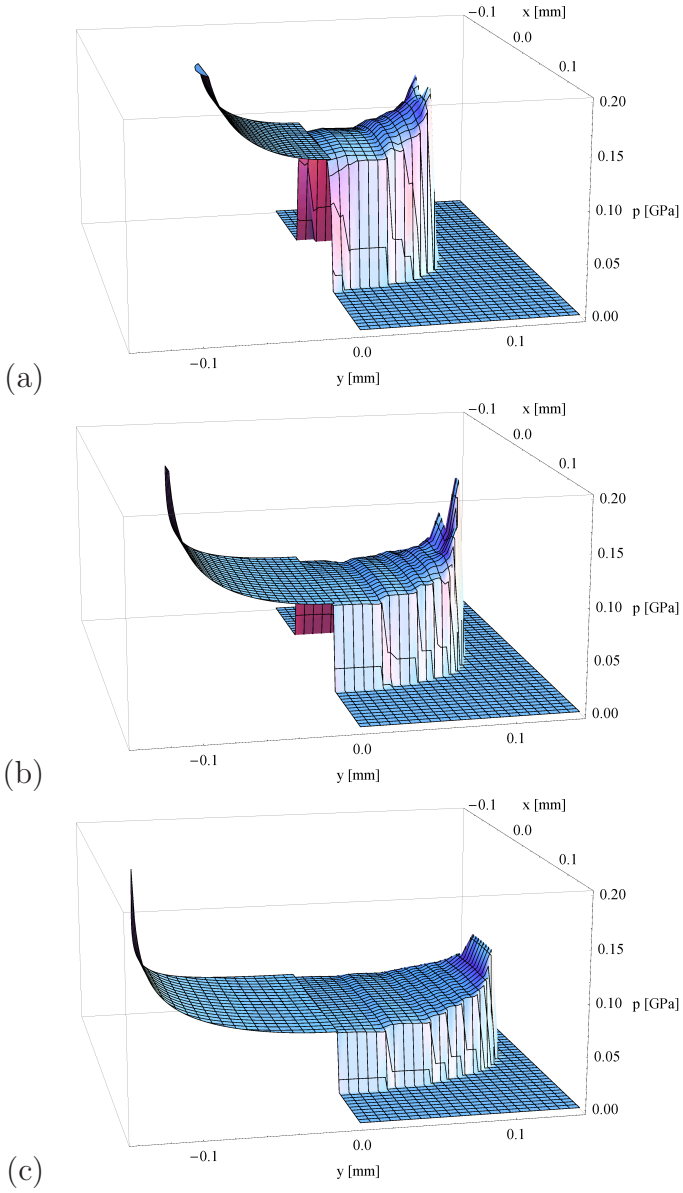

Figure 8: Distribution of the contact pressure after (a) 1200, (b) 2500 and (c) 5000 cycles. In each figure, the prediction of the rigid-wear model (left) is compared to the corresponding result of the 3D finite element model obtained for $F = 2$ N (right).

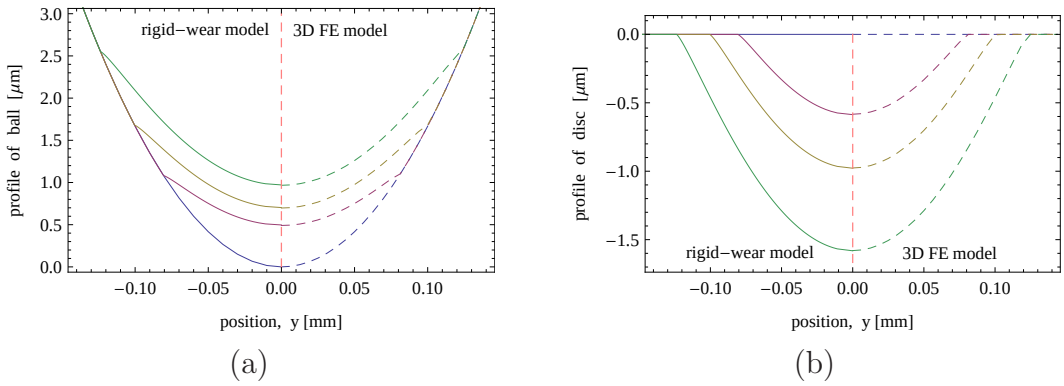

(a) (b)

Figure 9: Evolution of (a) wear scar on the ball and (b) wear groove on the disc at $x = 0$. Successive profiles correspond to 0, 1200, 2500 and 5000 cycles. In each figure, the prediction of the rigid-wear model (left) is compared to the corresponding result of the 3D finite element model obtained for $F = 2$ N (right).

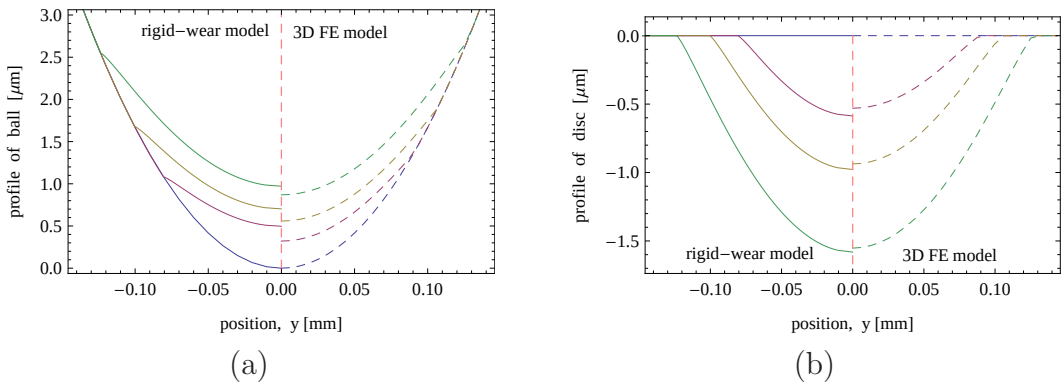

(a) (b)

Figure 10: Evolution of (a) wear scar on the ball and (b) wear groove on the disc at $x = 0$. Successive profiles correspond to 0, 1200, 2500 and 5000 cycles. In each figure, the prediction of the rigid-wear model (left) is compared to the corresponding result of the 3D finite element model obtained for $F = 20$ N (right).

force $F = 2$ N, the wear-controlled contact conditions are reached when the wear depth is about 1 μm, which is small compared to the ball radius of 3 mm. As expected, the transient period is longer for $F = 20$ N, but it is evident that contact evolves towards the wear-controlled conditions. Once the wear-controlled conditions are reached, all the essential features of the finite element solution, i.e. the wear profiles, the contact zone and the contact pressure, are accurately reproduced by the simple rigid-wear model at the computational cost that is 3–4 orders of magnitude lower (several seconds in the case of the rigid-wear model and several hours in the case of the finite element computations).

The peak pressure at the edge of the contact zone is the only feature that exhibits discrepancy between the two models. This deserves a comment. On one hand, it is evident from Fig. 8 that the resolution of the present finite element model is insufficient to accurately capture the local fields at the edge of the contact zone (of course, the accuracy can be improved by refining the mesh). On the other hand, the rigid-wear model certainly overestimates the peak pressure, and this prediction of the model must be taken with due caution, see also the discussion at the end of Section 4.2.

4.2. Parametric study

It follows from Section 2.5 that, upon introducing dimensionless quantities, the evolution of wear and contact pressure is fully described by a family of dimensionless solutions parameterized by the wear-mode index I_w. Accordingly, the response of the rigid-wear model is presented here for three values of $I_w = 4.77$, 47.7 and 477. The intermediate value of $I_w = 47.7$ corresponds to the parameters adopted in the study of Section 4.1. The specific values of the dimensionless time $\bar{t} = 1.5 \times 10^{-8}$, 2.3×10^{-7}, 1.5×10^{-6} and 5.8×10^{-6}, which are referred to in the examples below, correspond to 125, 2000, 12500 and 50000 cycles, respectively, again in the reference to the study of Section 4.1.

Evolution of the shape of the contact zone is illustrated in Figs. 11 and 12. It is seen that the high value of I_w, cf. Fig. 11c, results in an elongated shape of the wear scar, and the ratio $\bar{a}_0/\bar{L}$ decreases with increasing time, cf. Fig. 12c. This refers to the situation in which mostly the disc wears away. In contrast, for the low value of I_w, cf. Fig. 11a, the wear scar is nearly circular, and this refers to the situation in which mostly the ball wears away.

Figure 13 shows the maximum wear depth of the ball and of the disc, i.e. $\bar{w}_b^0(0,\bar{t})$ and $\bar{w}_d(0,\bar{t})$, respectively, and the total approach $\bar{H}(\bar{t}) = \bar{w}_b^0(0,\bar{t}) +$

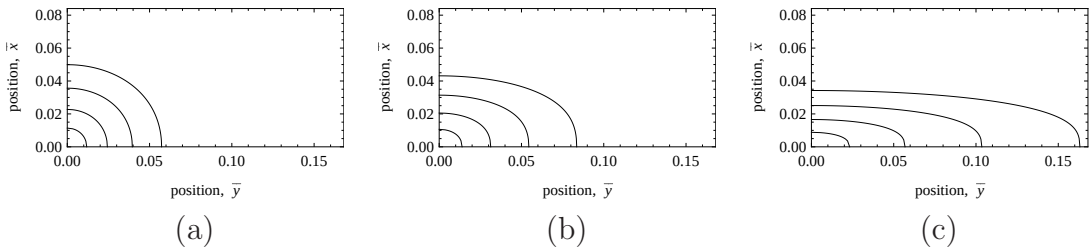

(a) (b) (c)

Figure 11: Evolution of the contact zone for: (a) $I_w = 4.77$, (b) $I_w = 47.7$ and (c) $I_w = 477$. Successive contours correspond to $\bar{t} = 1.5 \times 10^{-8}$, 2.3×10^{-7}, 1.5×10^{-6} and 5.8×10^{-6} (one quarter is only shown).

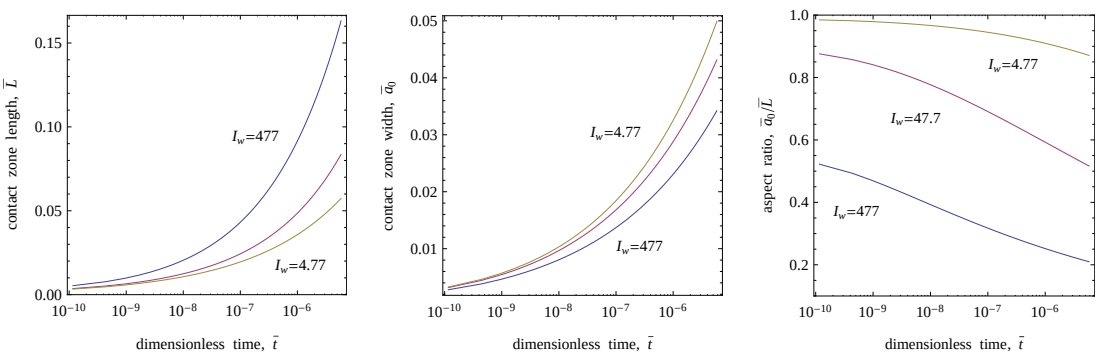

(a) (b) (c)

Figure 12: Evolution of the contact zone (a) half-width $\bar{L}$, (b) half-length $\bar{a}_0$, and (c) aspect ratio $\bar{a}_0/\bar{L}$.

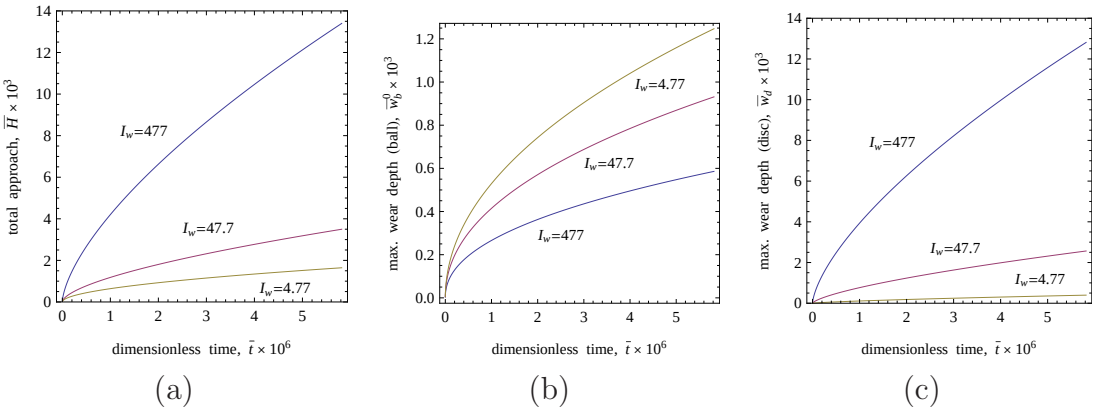

Figure 13: Maximum wear depth (a) of the ball $\bar{w}_b^0(0, \bar{t})$ and (b) of the disc $\bar{w}_d(0, \bar{t})$, and (c) the total approach $\bar{H}$ as a function of time.

$\bar{w}_d(0, \bar{t})$. As expected, the wear depth of the disc increases with increasing wear-mode index I_w. The influence of I_w on the wear depth of the ball is less obvious. Assume that k_d is varied and all the other parameters are kept constant. Then, the total wear volume of the ball at a fixed time is not affected by I_w, and the decrease of the wear depth of the ball with increasing I_w is related to the corresponding increase of the width of the contact zone, cf. Figs. 11 and 12a.

Evolution of the contact pressure is illustrated in Fig. 14. The model predicts that the pressure increases towards the edge of the contact zone $|y| = L$, and this feature is confirmed by the finite element computations, cf. Fig. 8. However, the maximum pressure is certainly overestimated by the present rigid-wear model, particularly for high I_w, because such a high pressure would be relaxed by local elastic deflections.

5. Conclusions

A computationally efficient model of evolution of wear in quasi-steady-state sliding contacts has been developed and applied to analysis of the pin-on-disc wear problem. The model is built on the assumption that contact conditions are controlled by the wear process only, and elastic deflections have a negligible effect on the solution. This condition is satisfied after a short initial period in which the elasticity effects gradually diminish. Validity of this assumption has been successfully verified using a full three-dimensional finite element model.

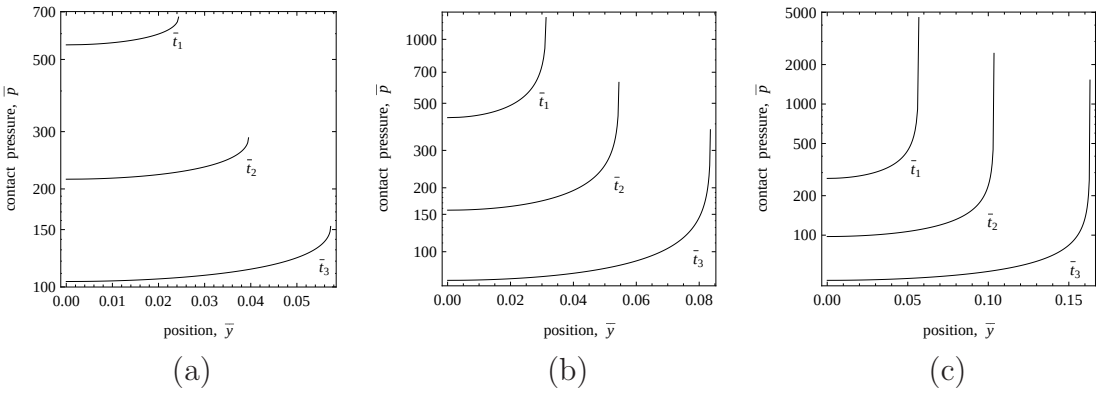

Figure 14: Evolution of pressure for (a) $I_w = 4.77$, (b) $I_w = 47.7$ and (c) $I_w = 477$ at selected time instants $\bar{t}_1 = 2.3 \times 10^{-7}$, $\bar{t}_2 = 1.5 \times 10^{-6}$ and $\bar{t}_3 = 5.8 \times 10^{-6}$.

Detailed analysis has been carried out for the case of the Archard wear model. Two computational schemes have been proposed, and a simple *Mathematica* code implementing these schemes is available to an interested reader, see the Appendix.

It has been shown that, upon introducing dimensionless quantities, evolution of contact and wear depends on a single dimensionless parameter, called the wear-mode index, which characterizes the relative magnitude of wear coefficients of the contact pair. Results of a parametric study are presented which illustrate the predicted evolution of the wear profiles, the contact zone and the contact pressure.

The approach can be easily extended to more complex local wear models, for instance, assuming pressure-dependence of the wear coefficient. In view of its simplicity and computational efficiency, the model is particularly suitable for identification of parameters of wear models using the pin-on-disc or reciprocating pin-on-flat wear tests.

Acknowledgement. This work has been partially supported by the KomCerMet project (contract no. POIG.01.03.01–14–013/08–00 with the Polish Ministry of Science and Higher Education) in the framework of the Operational Programme Innovative Economy 2007-2013.

Appendix A. Implementation in *Mathematica*

The two computational schemes introduced in Section 3 have been implemented in *Mathematica* (www.wolfram.com). The corresponding code is

provided as a supplementary material, and the *Mathematica* notebook can be downloaded from `http://www.ippt.gov.pl/~jleng/RigidWearModel/`.

The complete set of incremental governing equations is provided in Section 3. For completeness, we describe below the time incrementation scheme that has been adopted based on the experience gained in the course of development of the code. Specifically, we have observed that it is beneficial that the time increment is possibly small at the beginning of the wear process and then gradually increases so that the accuracy and the computational cost are balanced.

Assume that the total number M_{max} of cycles (e.g., revolutions of the disc) is given. In the following, the current number of cycles, denoted by M, is used as a measure of time, and we have $M = vt/S$. Denote by N_{ts} the prescribed number of time steps in the simulation. The increment ΔM_n at each time step $n = 1, \ldots, N_{ts}$ is assumed to increase according to:

$$\Delta M_n = n\alpha. \tag{A.1}$$

Parameter α is selected such that the sum of the increments $M_0 + \sum_n \Delta M_n$ is equal to M_{max} so that we have:

$$\alpha = \frac{2(M_{max} - M_0)}{(N_{ts} + 1)N_{ts}}. \tag{A.2}$$

As described in Section 3, in the implicit time integration scheme the initial number of cycles M_0 is set to 0, and $M_0 = V_{ini}/(k_b F S)$ in case of the explicit time integration scheme.

References

[1] J.F. Archard. Contact and rubbing of flat surfaces. *J. Appl. Phys.*, 24(8):981–988, 1953.

[2] L. Johansson. Numerical simulation of contact pressure evolution in fretting. *Trans. ASME J. Tribol.*, 116:247–254, 1994.

[3] N. Strömberg. An augmented lagrangian method for fretting problems. *Eur. J. Mech. A/Solids*, 16:573–593, 1997.

[4] P. Pödra and S. Andersson. Simulating sliding wear with finite element method. *Tribol. Int.*, 32(2):71–81, 1999.

[5] V. Hegadekatte. *Modeling and simulation of dry sliding wear for micromachine applications*. PhD thesis, Universität Karlsruhe, 2006.

[6] C. Paulin, S. Fouvry, and C. Meunier. Finite element modelling of fretting wear surface evolution: Application to a Ti-6A1-4V contact. *Wear*, 264:26–36, 2008.

[7] J. Lengiewicz and S. Stupkiewicz. Continuum framework for finite element modelling of finite wear. *Comp. Meth. Appl. Mech. Engng.*, 205-208:178–188, 2012.

[8] I. Serre, M. Bonnet, and R. M. Pradeilles-Duval. Modelling an abrasive wear experiment by the boundary element method. *C. R. Acad. Sci. Paris, Serie II b*, 329:803–808, 2001.

[9] G.K. Sfantos and M.H. Aliabadi. A boundary element formulation for three-dimensional sliding wear simulation. *Wear*, 262:672–683, 2007.

[10] L. Rodriguez-Tembleque, R. Abascal, and M. H. Aliabadi. Anisotropic wear framework for 3D contact and rolling problems. *Comp. Meth. Appl. Mech. Engng.*, 241–244:1–19, 2012.

[11] L. Gallego, B. Fulleringer, S. Deyber, and D. Nélias. Multiscale computation of fretting wear at the blade/disk interface. *Tribol. Int.*, 43:708–718, 2010.

[12] J. Andersson, A. Almqvist, and R. Larsson. Numerical simulation of a wear experiment. *Wear*, 271(11-12):2947–2952, 2011.

[13] P. Pödra and S. Andersson. Wear simulation with the Winkler surface model. *Wear*, 207(1–2):79–85, 1997.

[14] M. Peigney. Simulating wear under cyclic loading by a minimization approach. *Int. J. Sol. Struct.*, 41:6783–6799, 2004.

[15] I. Páczelt and Z. Mróz. On optimal contact shapes generated by wear. *Int. J. Num. Meth. Engng.*, 63:1250–1287, 2005.

[16] I. Páczelt and Z. Mróz. On the analysis of steady-state sliding wear processes. *Tribol. Int.*, 42(2):275–283, 2009.

[17] I. Páczelt, S. Kucharski, and Z. Mróz. The experimental and numerical analysis of quasi-steady wear processes for a sliding spherical indenter. *Wear*, 274–275:127–148, 2012.

[18] I.I. Argatov. Asymptotic modeling of reciprocating sliding wear with application to local interwire contact. *Wear*, 271(7-8):1147–1155, 2011.

[19] I.I. Argatov and W. Tato. Asymptotic modeling of reciprocating sliding wear – comparison with finite-element simulations. *Eur. J. Mech. A/Solids*, 34:1–11, 2012.

[20] J. Korelc. Automation of primal and sensitivity analysis of transient coupled problems. *Comp. Mech.*, 44:631–649, 2009.

[21] J. Lengiewicz, J. Korelc, and S. Stupkiewicz. Automation of finite element formulations for large deformation contact problems. *Int. J. Num. Meth. Engng.*, 85:1252–1279, 2011.